Superhydrophobic condenser surfaces for air gap membrane distillation

Citation: Warsinger, David E.M., Jaichander Swaminathan, Laith A. Maswadeh, and John H. Lienhard V. "Superhydrophobic Condenser Surfaces for Air Gap Membrane Distillation." Journal of Membrane Science 492 (October 2015): 578–587.

As Published: http://dx.doi.org/10.1016/j.memsci.2015.05.067

Publisher: Elsevier

Persistent URL: http://hdl.handle.net/1721.1/102500

Version: Author's final manuscript: final author's manuscript post peer review, without publisher's formatting or copy editing

Superhydrophobic Condenser Surfaces for Air Gap Membrane Distillation

David E. M. Warsinger[1], Jaichander Swaminathan[1], Laith A. Maswadeh[1], John H. Lienhard V[1*],

[1]Rohsenow Kendall Heat Transfer Laboratory, Department of Mechanical Engineering Massachusetts Institute of Technology, 77 Massachusetts Avenue, Cambridge MA 02139-4307 USA

[*]Corresponding Author lienhard@mit.edu

ABSTRACT

Superhydrophobic surfaces for enhanced condensation in Air Gap Membrane Distillation (AGMD) may provide significantly improved distillate production rates and increased thermal efficiency. While AGMD is one of the most thermally efficient membrane distillation desalination configurations, large transport resistances in the air gap limit distillate production rates. AGMD experiments were performed with combinations of untreated, hydrophobic, and superhydrophobic condensation surfaces. A nanostructured copper oxide coated condensing surface produced durable 164°±4° contact angles and jumping droplet condensation. Tests were also performed on the air gap spacer, in this case a small diameter support mesh, to judge the effects of superhydrophobic treatment and conductivity on distillate production for AGMD. A novel visualization technique was implemented to see through PVDF membranes and confirm air gap behavior. The experiments were compared with numerical modeling of AGMD film-wise condensation and flooded-gap MD. The results indicate that the introduction of superhydrophobic surfaces can result in improvements in distillate production in excess of 60% over standard AGMD. However, for high distillate production condensation on the superhydrophobic plate transitions from a partially wetted droplet morphology to Wenzel flooded (wetting) conditions. Mildly hydrophobic condensing surfaces were found to provide moderate improvement in distillate production. Superhydrophobic support meshes made a negligible difference in distillate production, but high conductivity support meshes showed significant increases in flux at the expense of thermal efficiency. The results outline recommended superhydrophobic condensation conditions at varied feed and cold side temperatures for substantial improvement to distillate production rate for AGMD systems in a flat plate configuration.

KEYWORDS

membrane distillation, desalination, superhydrophobic surface, jumping droplets, heat transfer enhancement

NOMENCLATURE

c	concentration [mol/m^3]
d	channel depth [m]
d_{gap}	air gap width [mm]
D_{wa}	Diffusivity of water in air [m^2/s]
J	mass flux [kg/m^{2}s]
k	conductivity [W/m K]
L	module effective length [m]
$\dot{m}$	mass flow rate [kg/s]
M	molecular weight [kg/kmol]
n	discretized cell
p	partial pressure [Pa]
q	heat flux [W/m2]
T	temperature [C]
x	mole fraction [-]
z	distance along module length [m]
δ	thickness of condensate film [m]
ρ	density [kg/m^3]
$(\cdot)_{\text{a}}$	air
$(\cdot)_{\text{b}}$	bulk/free stream
$(\cdot)_{\text{f}}$	feed
$(\cdot)_{\text{i}}$	air-liquid interface
$(\cdot)_{\text{m}}$	membrane
AGMD	Air Gap Membrane Distillation
EES	Engineering Equation Solver

MD Membrane Distillation

PVDF Polyvinylidene Fluoride

PW Partial Wetting

W Wetting

1. INTRODUCTION

1.1 Membrane Distillation and Droplet Condensation

Membrane distillation (MD) is a quickly advancing thermal desalination technology capable of providing low-maintenance water filtration using waste-grade or renewable heat. Membrane distillation units show promise for desalination on both the small and large scale and unlike reverse osmosis, are fouling resistant and have performance minimally affected by increases in salinity [1]. Recent work has suggested MD can potentially have similar or superior efficiencies to other state-of-the-art thermal desalination technologies as well [2, 3, 4]. Air Gap Membrane Distillation (AGMD) is an MD configuration with an air-filled cavity between the membrane and condensing surface. The thermal resistance of the air gap reduces conduction heat loss between the cooling surface and hot feed, and hence sustains the driving force for vapor transfer through the membrane. This comes at the cost of a large associated mass transfer resistance to vapor diffusion across the air gap [5]. Among implemented MD configurations, Summers et al. [6] has shown that AGMD is capable of the highest energy efficiency.

Two basic droplet morphologies exist for drop-wise condensation on microscopically rough surfaces: wetted and suspended. The wetted morphology, also known as a Wenzel droplet, adheres to the surface and grows rapidly. Water infiltrates the rough surface under the droplet, pinning it to the surface [7] and allowing for enhanced conduction through the surface and droplet [8]. Droplets can then grow to a large size before shedding due to gravity. The suspended morphology, also known as a Cassie-Baxter droplet, forms on top of surface features and leaves the surface non-wetted. This leads to lower conduction through the surface and slower growth, but also allows droplets to detach from the surface more easily and at smaller sizes [9, 10]. Jumping droplet condensing occurs in a partial wetting morphology, where a small wetted region develops on a nucleation site and grows into a droplet which is suspended over the surface features around that site. The behavior of partial wetting varies based on surface geometry, nucleation density, and local energy barriers [11]. Studies have shown that surfaces with higher contact angles tend to form smaller droplets that de-pin and jump from the surface more readily, leading to enhanced heat transfer [12]. It is the combination of rapid growth from partial wetting and the rapid ejection of droplets that enhances heat transfer: extremely pinned droplets cause flooding which often impedes overall heat transfer.

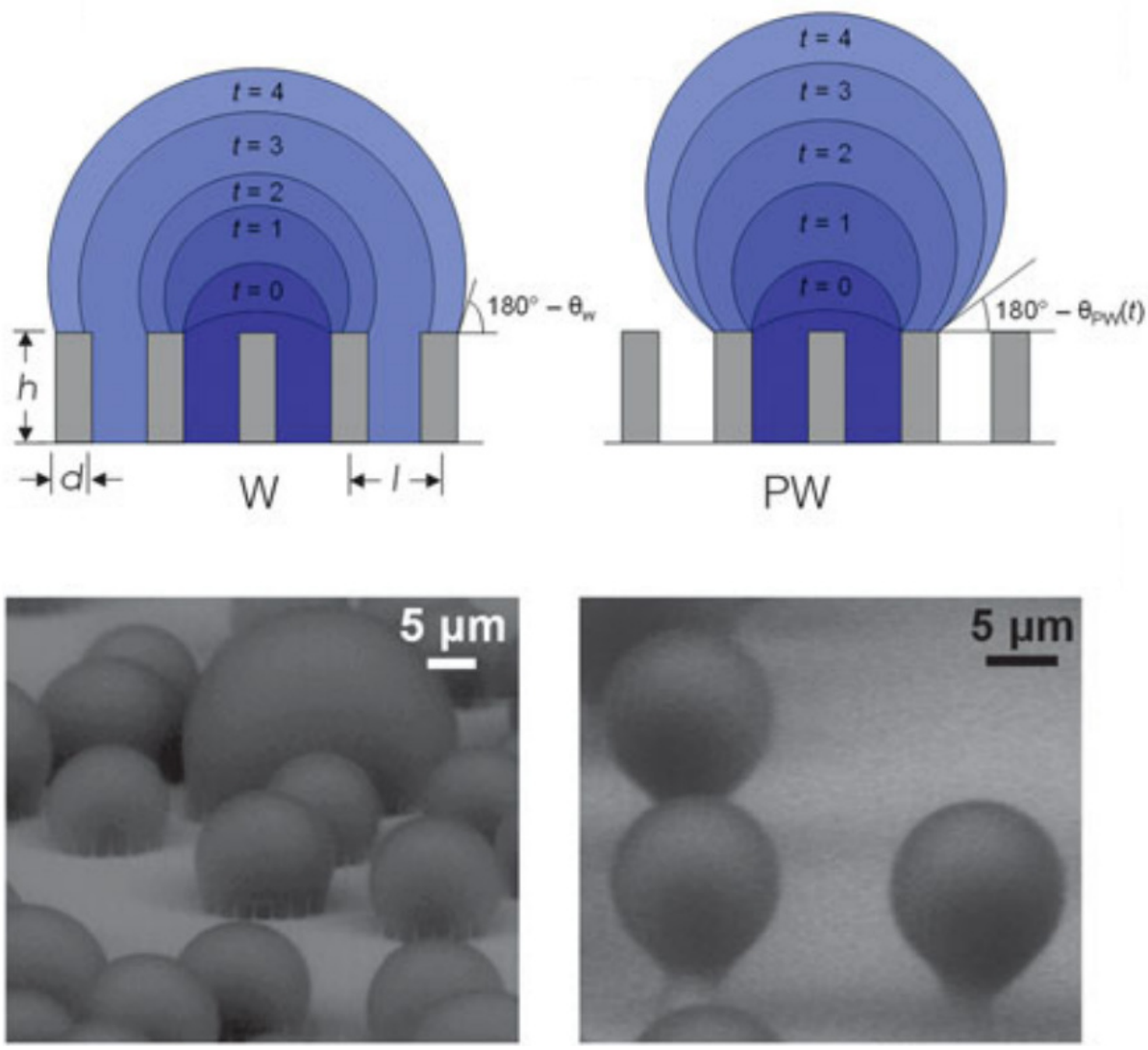

Fig. 1 Left, top and bottom: diagram and ESEM image of Wenzel droplet (flooded) condensation, and right, top and bottom, partially wetting droplet diagram and ESEM image, modified from [11]. A suspended droplet regime, not pictured, resembles partially wetted, but with no liquid water between the surface features.

Partially wetted droplets as seen in Fig. 1 have the advantage of improved thermal conductance between the droplet and surface, allowing for better heat transfer and faster nucleation and jumping. The copper oxide surfaces used here and in previous studies are designed specifically for that purpose [11].

1.2 Condensing in AGMD

Several condensing regimes may occur in AGMD, depending on the condensation rate, air gap width, module height, and surface hydrophobicity among other parameters. Traditional AGMD simply condenses distillate in the laminar film regime, an understood and well-characterized process [13, 14]. With superhydrophobic surfaces, jumping droplets may occur, especially at low distillate flow rates and

small air gap thicknesses. In this regime, small droplets combine and eject from the surface, with droplet sizes in the range of ≈10−100 μm [11].

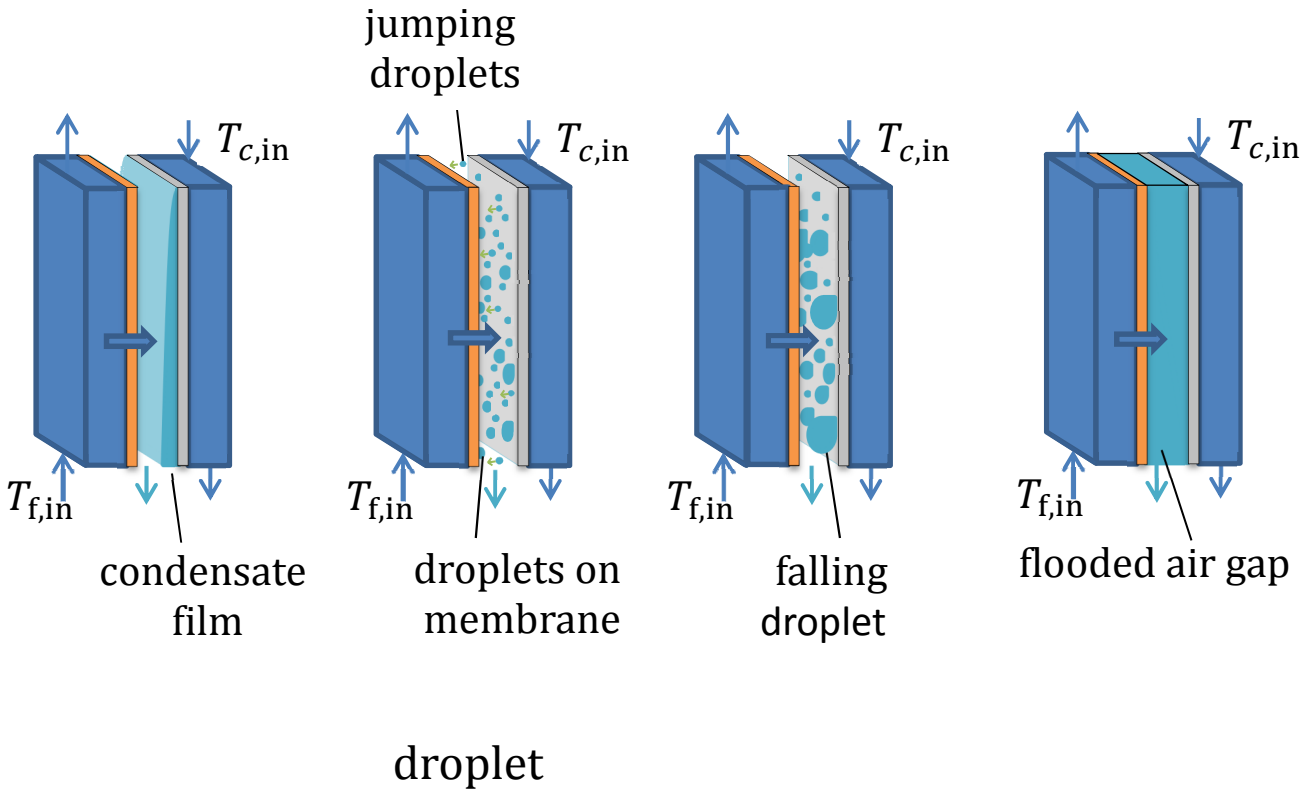

Fig. 2 Diagram of condensation regimes that may occur in AGMD.

AGMD systems normally operate in a film condensation mode on the condenser surface. Recent research work in condensing surfaces has focused on drop-wise condensation on hydrophobic surfaces, which can have five to seven times the heat transfer coefficient of laminar film condensation [11]. Jumping droplet condensation on superhydrophobic surfaces provides further heat transfer coefficient improvement: for the coatings used in this study, previous work has shown a 25% increased heat flux and a 30% increased condensation heat transfer coefficient compared to state-of-the-art hydrophobic surfaces [15]. The jumping phenomenon is a result of the fusion of small droplets (10−100 μm) leading to a decrease in total surface area. The reduction in surface energy translates into a release of kinetic energy through a dynamic instability as the smaller droplets coalesce, which can launch the droplet from the surface [15]. The silanized copper oxide (CuO) surface used in this study produces a durable superhydrophobic surface which may provide a low-cost, scalable method for industrial use of drop-wise condensation.

The combination of superhydrophobic surfaces and membrane distillation, a novel implementation developed in this work, may provide significantly increased efficiency and condensate production rates for AGMD desalination. A flat plate AGMD module was designed for use with interchangeable condenser plates with different surface treatments. Two distinct behaviors were seen

in superhydrophobic condenser testing. At lower rates of distillate flux, jumping droplet condensation was measured and observed and at higher rates of flux, flooding was seen to occur. The module also used a replaceable mesh air gap spacer and several mesh options were tested for effects on performance. It was found that mesh hydrophobicity had a small impact on distillate production but mesh conductivity could have a significant effect on distillate production. Experimental results were compared to a model of the system which used a finite difference analysis for film-wise condensation. The model accurately represented the film-wise AGMD tests and flooded conditions, with the jumping droplet results falling in between the two but closer to the flooded results.

2. METHODS

2.1 Experimental Set-up

An air gap membrane distillation apparatus was constructed alongside a finite difference Engineering Equation Solver (EES) model [16]. The system was designed to minimize temperature change in the feed solution (<0.5°C) as it flows across the feed channel, allowing for fine control of conditions within the AGMD module.

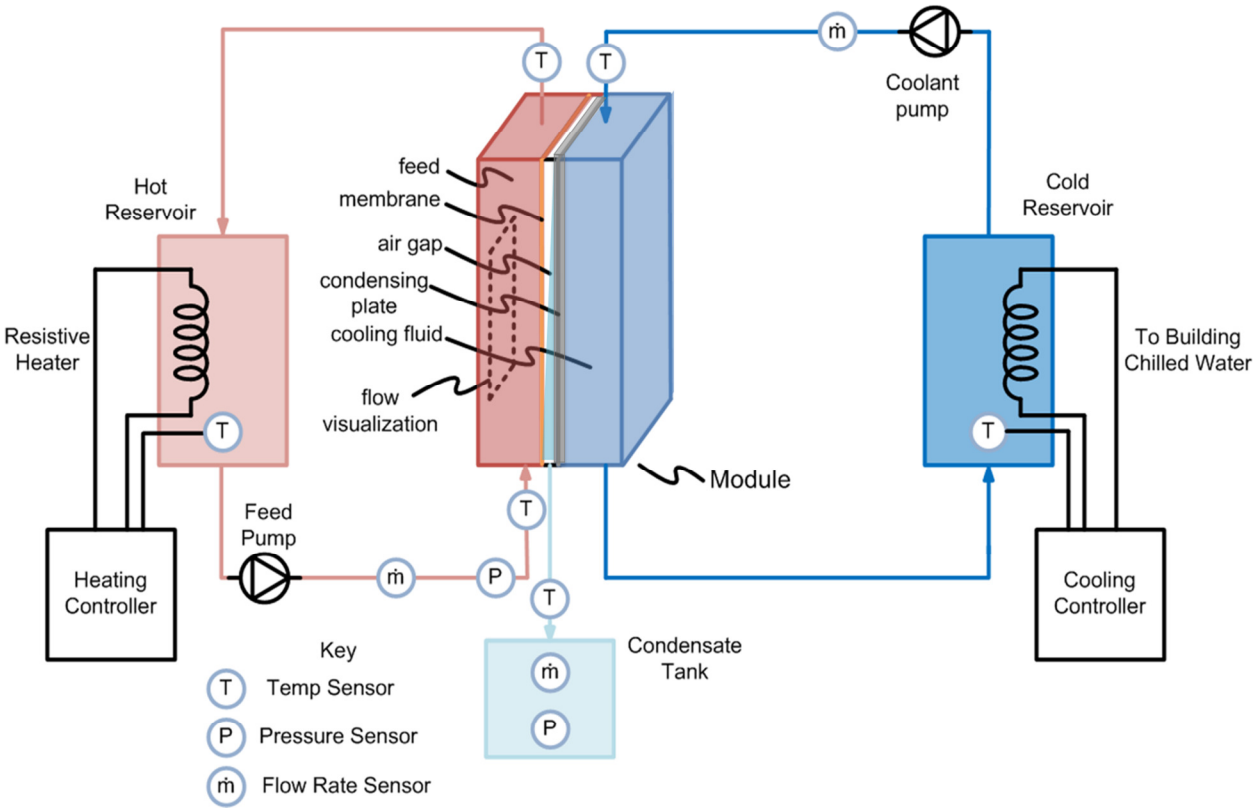

Fig 3. AGMD Apparatus diagram for superhydrophobic condensing and control tests

The system consists of a flat plate AGMD module connected to heating and cooling loops. The heating and cooling systems each contain a large tank with resistive heating elements connected to a temperature controller. The cold tank also connected to a cold water feed for testing at temperatures as low as 10 °C, and both tanks were sized to maintain consistent temperatures for the module feeds. Temperature and flow rate were measured at various points in the heating and cooling loops, including the entrances and exits of the module feed channels. Additionally, a small condensate collection tank was used to collect distillate and an electronic mass scale under this tank measured the mass flow rate of condensate. Components were chosen with temperature tolerances designed for a set range of operating conditions from 20°C to 90°C for the hot feed and from 10°C to 70°C for the cold side.

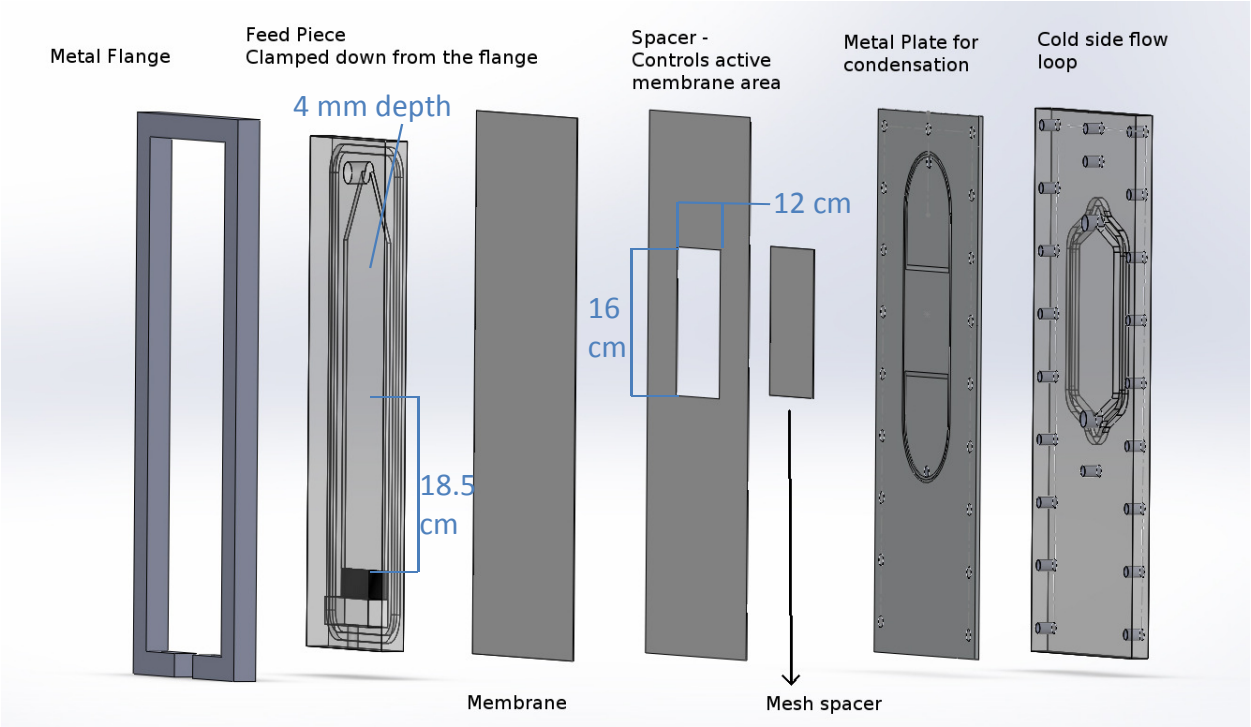

Fig. 4 Membrane distillation apparatus module diagram. The flow channels are machined into polycarbonate or aluminum plates. Dimensions for the feed developing flow region (16 cm) and the active membrane area is shown.

The air gap module itself was constructed with a series of close-tolerance, CNC machined plates. The feed and cooling channels are milled into clear polycarbonate blocks, and the feed channel is longer than the active membrane area in order to ensure fully developed turbulent flow over the exposed membrane. An aluminum plate with a recessed collection region conducts heat from the condenser to the cold water feed and holds the copper condensing plate in the air gap. A small support mesh between the membrane and condenser plate maintains the air gap spacing.

The air gap size and system conditions were designed to maximize distillate flux. Repeatability experiments were performed for some of the trials to ensure reliable results, one of which is included here. More details are in the uncertainty analysis section. Influences from previous tests were eliminated by total dry out of the system (> 24 hours) between tests. To ensure stable conditions, each test was allowed to stabilize for at least 15 minutes before data was taken: this time frame was chosen because results showed stabilization of flux well within this. Tests were run starting at low temperature and continuing to high temperature, to avoid any effects from high temperature flooding. (The one exception is mentioned elsewhere in the paper. The air gap sizes used were on the smaller side of typical systems. Optimized systems that maximize distillate flux have smaller gap sizes in this range [17], often on the order of 1 mm.

Variables	Symbol	Experiment Values	Control
Feed temperature	$T_{f,in}$	30-80 °C	±0.1°C
Feed flow rate	$m_{f,in}$	0.25 kg/s	±0.003 kg/s
Coolant temperature	T_c	10-50°C	±0.5°
Coolant flow rate	$m_{c,in}$	0.2 kg/s	±0.003 kg/s

Table 1 Operating ranges and tolerances of variable parameters during testing

System Parameters	
Air gap	
Thickness	0.45-2 mm
Pressure	1 atm
Active Membrane Area	6.3”x 4.72”
Feed Channel	
Turbulent, fully developed	
Length	16 cm
Width	12 cm
Height	4 mm

Table 2 Air gap and feed channel parameters

Measurement	
Device	Uncertainty
Thermistors	±0.1°C
scale (distillate)	±0.1 g

Table 3 Measurement uncertainty of instruments

2.2 Uncertainty Analysis

The uncertainty in experimental flux measurements is evaluated by considering the uncertainty in mass scale measurement (±0.1 g) and the total uncertainty in time (±10 seconds) and their effect on the effective uncertainty in flux measured.

Uncertainty evaluation for the numerical modeling results was calculated with the Engineering Equation Solver model. Uncertainties in flow rate, pressure, dimensions, membrane permeability, and temperature were all included in the analysis. The dominant sources of uncertainty were variations of the temperatures in the feed and cooling channels. The feed temperature on-off controller controls temperature within a range ±0.1 °C within the set point temperature, whereas the cold stream inlet temperature varies ±0.5 ℃ around the set point value. In addition to this variation, there is an uncertainty associated with differences between the measured temperature and the actual bulk fluid inlet temperature, especially in the case of the hot feed water input (1 °C). As a result this uncertainty (1 °C) was used as the estimated uncertainty in the feed inlet temperature. The B value (permeability) of the membrane is not likely to be constant over the entire range of temperatures, and so an uncertainty of 5% was assigned. The overall uncertainty in flux evaluated by the model is shown (Fig. 11) at the highest and lowest temperature conditions in both air gap and water gap operating conditions and is found to be less than 6%. Repeatability experiments for select cases confirmed the accuracy of the system.

2.3 Superhydrophobic Coating

The superhydrophobic surface used for the condenser plate in this experiment is a silanized copper oxide (CuO) nanoscale surface which was found to provide a 25% higher heat flux and 30% higher condensation heat transfer coefficient than conventional copper at low supersaturation.

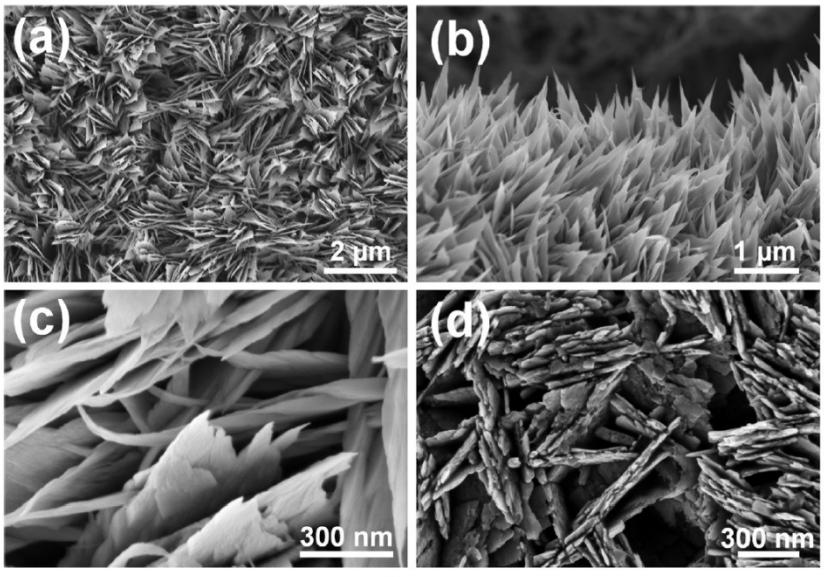

Fig. 5 The field emission scanning electron microscope (FESEM) images above show the copper oxide nanostructure surface from the top view (a), side view (b), and close up on the oxide "blades" without

the silane coating and the blades after they have been silanized (d). The resulting surface has an average height of ≈1 μm, a solid fraction of ≈2-3%, and rugosity (area ratio) of ≈10 [15].

As shown by Fig. 5 above, the surface is covered in nanoscale copper oxide blades which allow for selective nucleation of partially wetted (PW) droplets and high nucleation densities.

The superhydrophobic surface was created through a low temperature, self-limiting process developed by the E.N. Wang group at MIT [15]. A polished, copper alloy plate (Alloy 110, 99.9% pure) was cleaned in an ultrasonic bath of acetone for 10 minutes and rinsed with deionized water, ethanol, and isopropyl alcohol. The plate was dipped in a 2.0 M HCl bath for 20 minutes to remove the surface oxide layer before being rinsed with deionized water and dried with pure nitrogen gas.

The plate was then immersed in a 96±3 °C solution of $NaClO_2$, NaOH, $Na_3PO_4 \cdot 12H_2O$, and deionized water (3.75:5:10:100 wt%) in order to create the copper oxide nanostructure. This process creates a thin layer of copper (I) oxide, Cu_2O, which then re-oxidizes into the sharp copper (II) oxide, CuO, nanostructure.

Fluorinated silane (trichloro (1H,1H,2H.2H-perflouroоctyl)-silane) was then deposited from the vapor phase onto the CuO nanostructured surface to give the plate its hydrophobic character without changing the surface morphology [15].

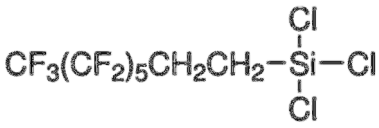

Fig. 6 Coating molecule used for hydrophobicity: Fluorinated silane (trichloro (1H,1H,2H.2H-perflouroоctyl)-silane).

For the experiments where the membrane support mesh was made hydrophobic, a commercial silicon-based superhydrophobic surface spray, Neverwet®, was used to coat the mesh. Neverwet is applied in two coatings of different roughness which results in a relatively robust superhydrophobic coating with a contact angle between 160 and 175° [18]. The mildly hydrophobic control surface included the silane coating, but not the rough copper oxide surface. The hydrophilic control surface was polished copper, which was also the substrate for the other surfaces. These surfaces represent realistic heat exchanger surfaces for thermal engineering systems.

2.4 Modeling

The experimental system's performance was predicted with numerical modeling using Engineering Equation Solver (EES). As modeling work has been previously published [6], only variations

of the model will be examined here. The model calculates one dimensional transport of mass and energy across a unit cell, with about 400 unit cells used to describe the experimental system. The model takes input parameters including Reynolds number, bulk temperature and mass flow rate of the hot side feed, and condenser temperature and calculates a variety of parameters including Nusselt numbers, Sherwood Number, Schmidt number, effective conductivities, condensation film thickness, diffusion, thermal resistances, and MD membrane flux. The modeling includes concentration and temperature polarization effects in the feed channel near the membrane surface. The diagram below shows the temperature gradient of the hot side feed near the membrane surface.

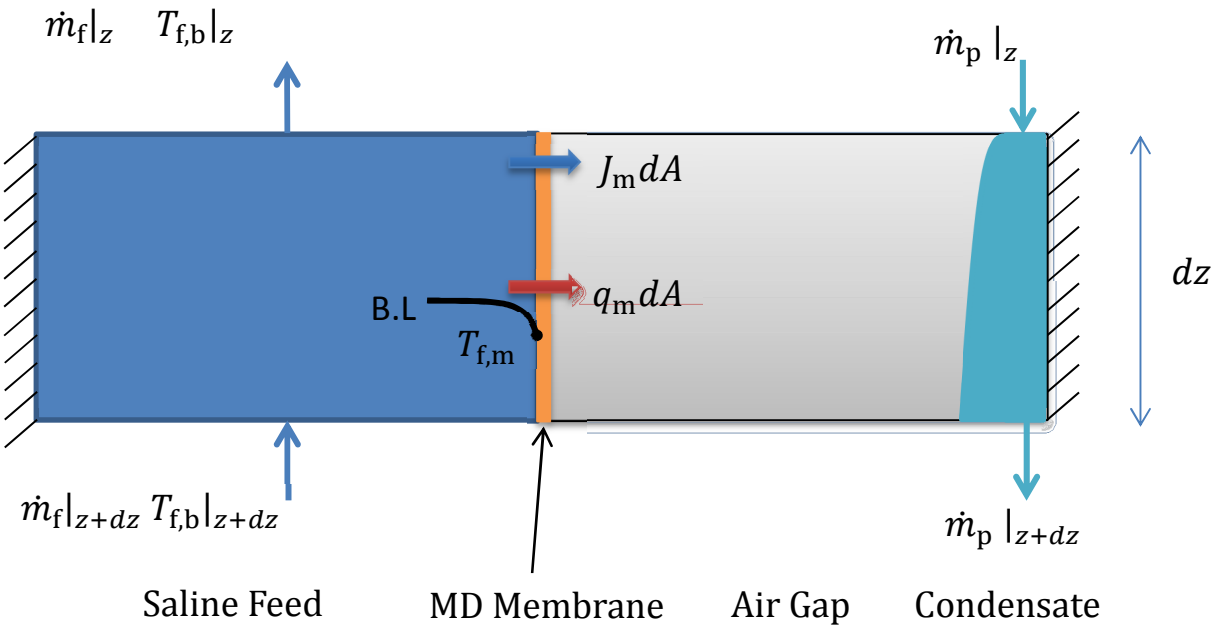

Fig. 7 Unit Cell for AGMD EES Numerical modeling, depicting conservation of mass and energy for each of the several hundred cells

The model assumes incompressible, fully developed flow, and uses the finite difference method. Diffusion of water vapor through the membrane in MD is generally modelled as a linear function of the vapor pressure difference across the membrane, with the membrane coefficient B:

$$J = B \times \left(P_{vap,f,m} - P_{vap,a,m}\right) \qquad (1)$$

In MD membranes, diffusion and Knudsen flow resistances can affect the *B* value [19]; however, the above flux equation has been supported by modeling and experiments.

The film condensation resistance is given by

$$q_c[n] = \frac{k_{\text{film}[n]}}{\delta[n]} \cdot \left(T_i[n] - T_{\text{wall}}[n]\right) \qquad (2)$$

where q_c is the heat flux, k_{film} is the conductivity of the condensate film, δ is the local condensate film thickness, T_i is the local membrane temperature, and T_{wall} is the local wall temperature [20]. Heat transfer due to the enthalpy of evaporation also occurs as water vapor is advected through the gap, and is given by

$$T_{a,m} - T_i = \left(\frac{q_{gap}}{k_{gap}}\right)\frac{\alpha\rho}{J}\left[\exp\left(\frac{J}{\alpha\rho}\left(d_{gap} - \delta\right)\right) - 1\right] \qquad (3)$$

where q_{gap} is the heat transfer across the gap, k_{gap} is the average thermal conductivity of the gap, d_{gap} is the air gap width, ρ is the density, α is the thermal diffusivity, and T_m is the temperature of the gap side of the membrane.

This model has previously been validated with experiments [21], and further validation was performed by the authors as seen in previous publications [22].

While the model is well understood and was validated for film condensation, which occurs on typical hydrophilic surfaces, two-phase flows with droplets on hydrophobic surfaces are difficult to model due to significant variation and complexity in flow and regime. Therefore, the results of previous film condensation experiments and models, as well as the results of well-characterized flooded gap models, were compared to the present superhydrophobic condensation experiments. The modeling indicates the lower and upper limits for the flux of the system, as a function of the effective mass transfer resistance of the gap decided by the droplet configuration.

Several parameters of the system differ significantly in drop-wise condensation. The condensation resistance decreases dramatically, as the droplets have a greater surface area to volume ratio, shed at smaller diameters, and exit the system more quickly than films. Drop-wise condensation has heat transfer coefficients five to seven times higher than film conduction in pure vapor conditions [23]. This heat transfer in this case can be described as:

$$q_c[n] = h_{eff} \cdot \left(T_{a,m}[n] - T_{wall}[n]\right) \qquad (4)$$

where h_{eff} is the effective heat transfer coefficient between the membrane surface and the wall. This heat transfer coefficient is affected by both the transfer in the gap as well as across the water on the surface. If transfer across the gap is restricted to diffusion as in AGMD, a smaller diffusion distance would lead to a higher transfer coefficient. At the same time, a larger liquid thickness on the plate would result in a lower transfer coefficient for conduction across the liquid.

The water vapor diffusion equation through the air gap between the membrane and the condensing surface is modeled as follows in the AGMD model:

$$\left(\frac{J[n]}{M_{H_2O}}\right) = \frac{c_a[n] \cdot D_{wa}}{d_{gap} - \delta[n]} \cdot ln\left(1 + \left(\frac{x_i[n] - x_{a,m}[n]}{x_{a,m}[n] - 1}\right)\right) \qquad (5)$$

where J_m is the flux through the membrane, M_{H2O} is the molecular weight of water, c_a is the local molar concentration of air, D_{wa} is the diffusivity of water in air, d_{gap} is the air gap depth, δ is the local condensation film thickness, x_i is the concentration of water vapor at the film-air interface, and $x_{a,m}$ is the local water mole fraction at the membrane interface [24]. The effective gap width d_{gap}-δ has a major effect on the heat and mass transfer resistances.

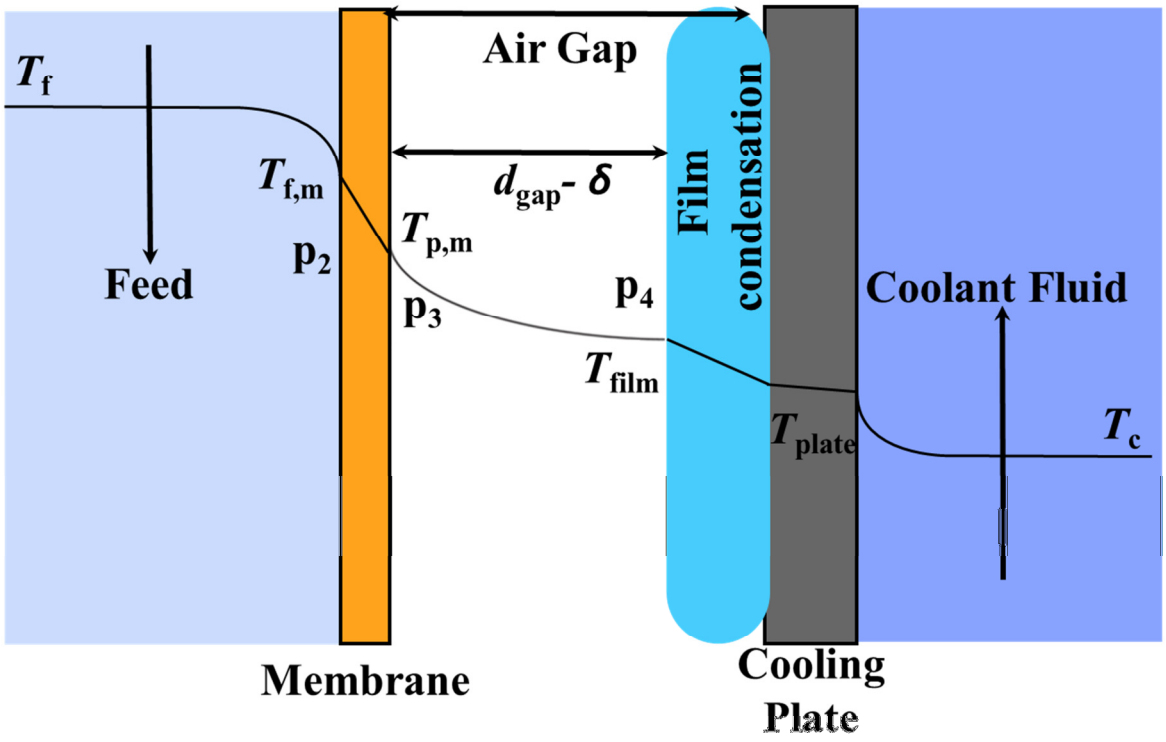

Fig. 8 Temperature profile of film wise AGMD, roughly proportional to the model

As seen from the temperature profile in Fig. 8, significance temperature gradients exist in the film condensation interface and the membrane. The main driving force for distillate production in MD is the temperature difference across the membrane. As heat transfer across a temperature gradient generates entropy, a significant temperature difference in any other region of the diagram, such as the condensate film, represent inefficiency. Drop-wise and jumping droplet condensation may reduce both the thermal resistance associated with conduction through a liquid film and the transport resistances in the air gap. These effects would each serve to increase distillate production.

2.5 Novel Visualization Technique for Validation

Visualization through the PVDF membrane was used to validate assumptions on the flow regime transitions occurring in superhydrophobic condensation experiments. In the module designed for this

research, clear polycarbonate allowed the membrane to be seen clearly through the hot side feed channel, but the air gap was not visible behind the membrane. Though plastics such as PVDF are transparent at low thicknesses, MD membranes are generally opaque due to the presence of surface features which cause absorption and scattering of visible light. Regions of the membrane were made transparent by melting at low temperature in order to remove surface features and pores in the material.

A soldering iron with electronic temperature control was set to 3 °C above the melting point of the PVDF material used, and applied with moderate pressure (~50 kPa). Some trial and error was required to develop a technique which did not puncture the membrane. Seven visualization regions were successfully incorporated into one membrane without breakthrough.

The visualization technique was used to observe jumping droplet condensation and large pinned droplets (flooding) occurring in the flow rate regimes claimed in the paper. Through the transparent windows in the membrane, jumping droplet condensation was observed for lower distillate flow rates and validates the improvement seen over conventional AGMD in this regime. Larger pinned Wenzel droplets were visible at higher flow rates and partial flooding likely explains the improvement in flux over film-wise AGMD in these tests.

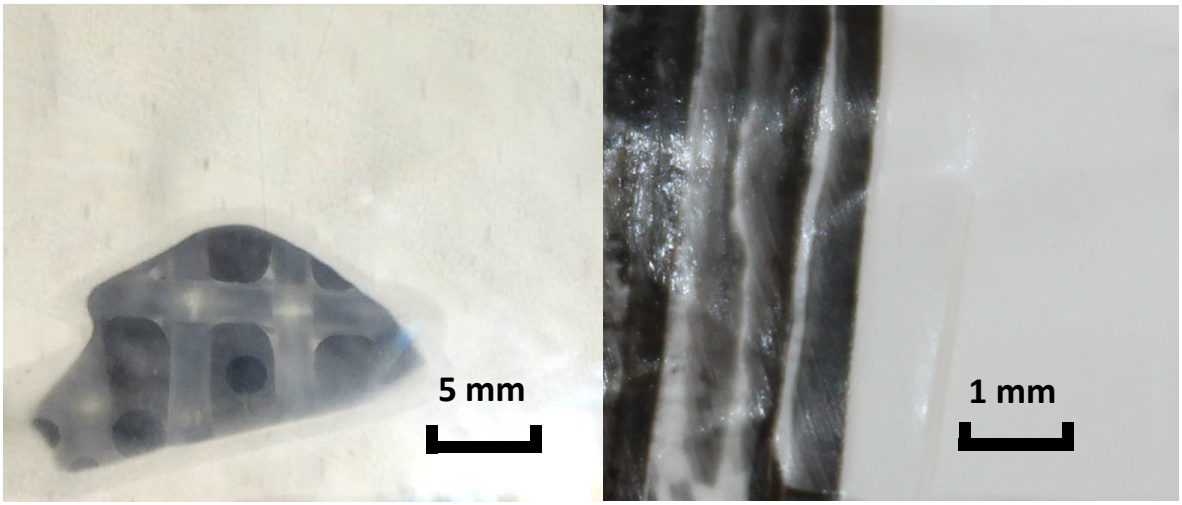

Fig. 9 Images of a transparent region of membrane developed for visual confirmation of air gap behaviors. The image on the left shows partial flooding occurring at high temperatures while the image on the right shows jumping droplet surface at lower temperatures. An iPhone 5s camera (left) and an EOS Rebel T3i Canon digital camera (right) were used.

3. RESULTS AND ANALYSIS

3.1 Experimental Results

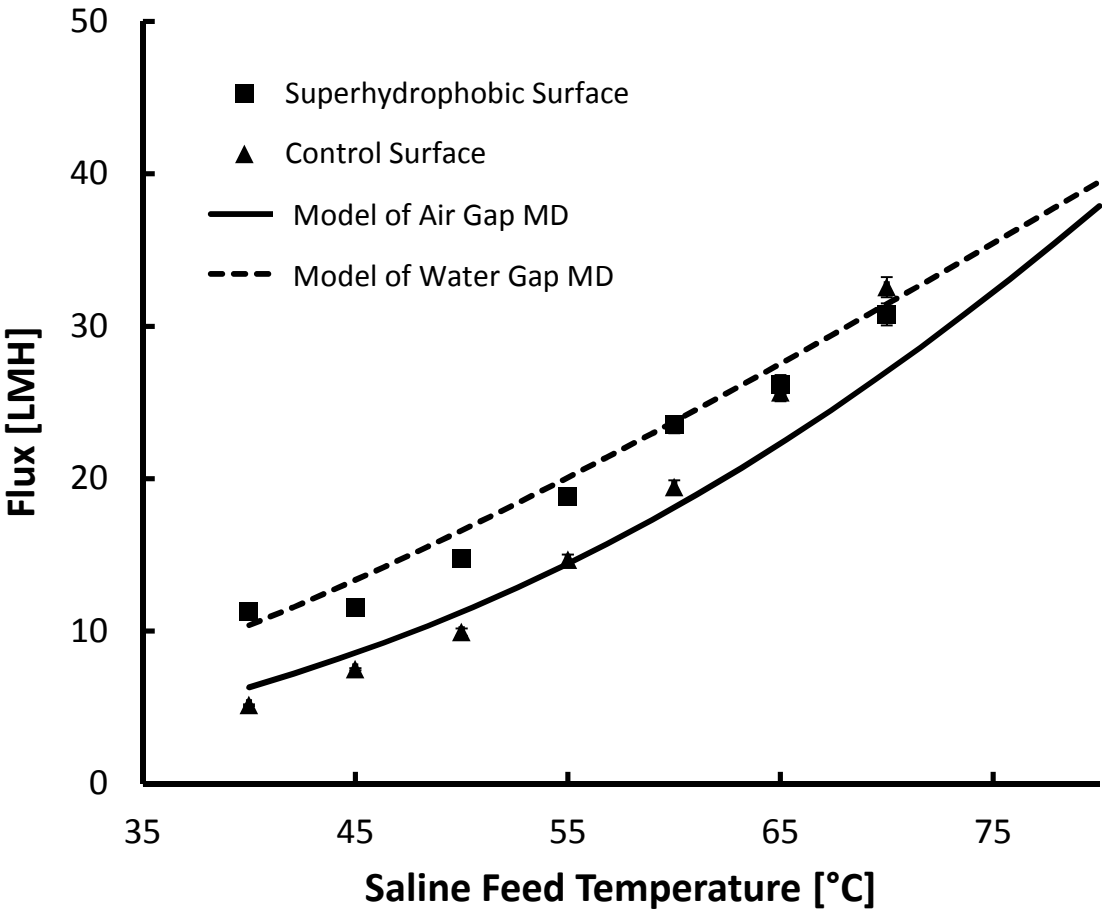

Fig. 10 Superhydrophobic and control surface AGMD experiments with 0.45mm air gap and 13°C cold side temperature. At lower temperatures, flux improvement with the superhydrophobic surface was very significant; ~119%. A model of ordinary AGMD, as described in the modeling section, predicts the control surface tests accurately at lower temperatures, though at temperatures above 65°C flooding begins to occur within the module. The performance of the superhydrophobic surface is similar to that of a water-filled gap, with lower mass transfer resistance.

Table 4. The uncertainty evaluation from the model for air gap and water gap configurations. The relative contribution of the different measured parameters is also included. The hot feed inlet temperature uncertainty is the major contributor in all cases. In the case of water gap, the effects of uncertainties in B value are higher than in the case of water gap.

Variable ± Uncertainty		B	$m_{c,in}$	$m_{f,in}$	$T_{c,in}$	$T_{f,in}$	$\underline{J}_{tot}$
[Units]		[kg/m^{2}Pa-s]	[kg/s]	[kg/s]	[°C]	[°C]	[kg/m^{2}hr]
Air Gap	T_H = 40°C	1.6E-6 ± 8.0E-8	0.2315 ± 0.005	0.2175 ± 0.005	13 ± 0.5	40 ± 1	6.313 ± 0.4182

Water Gap			0.1809 ± 0.005	0.2175 ± 0.005			10.39 ± 0.6333
Air Gap	T_H = 70°C		0.2315 ± 0.005	0.2175 ± 0.005		70 ± 1	27.02 ± 1.048
Water Gap			0.1809 ± 0.005	0.2175 ± 0.005			31.53 ± 0.8886

The first AGMD hydrophobicity trial performed with a small air gap (~0.45 mm) and constant cold side temperature of 13°C showed a dramatic increase in flux with superhydrophobic condensation, especially at lower temperature differences. While the flux was 120% higher for a temperature difference of 27°C, at 53°C temperature difference, it was nearly identical to the control experiment. Figure 10 plots the results from the superhydrophobic as well as control surface experiments. The results are compared against numerical modeling predictions of flux for AGMD and water filled gap MD scenarios which are likely to be the lower and upper limits respectively for the flux. The R^2 value for the fit between the control surface and the AGMD model is 0.92. The value is reduced by the transition from air gap to flooded behavior observed for the control experiment at a saline feed temperature of around 65°C. The R^2 fit value for the superhydrophobic experimental data and water gap model predictions is 0.97. Observations with the visualization method showed that the initial, lower temperature regime involved superhydrophobic jumping droplet condensation, and the later, reduced flux regime had a mostly flooded water gap. Both the modelled water gap and experimental superhydrophobic condensing exhibit a relatively small mass transfer resistance in the gap, making their condensate flux production similar.

The CuO superhydrophobic surface was designed for partial wetting condensation, and has two observed regimes from this and previous experiments. First, superhydrophobic condensing can create small jumping droplets which eject from the surface after combining with nearby drops. This mode is known to have superior heat transfer coefficients and condensation rates, as was the case for the low temperature- difference experiments. The other mode is flooding, in which the gaps between the microstructured features of the CuO surface become filled with water. As a result, wetted droplet condensation occurs, where the droplets grow to larger sizes and only shed by gravity. These droplets become highly pinned to the microstructured surface, and do not de-pin until they reach a larger diameter (~2-3mm [25]) than for smooth hydrophobic surfaces. Thermodynamically, this is similar to a condensate flooded gap. A water-filled gap has higher heat transfer between the hot and cold streams than an air-filled gap.

The system compares favorably to literature reported values for flux. It exceeds the large majority of studies examined in recent reviews [1], and for similar conditions, is of similar magnitude to the optimized maximum flux reported by Khayet et al. for AGMD [17]. Their study reported AGMD flux of 47 LMH compared to 56 LMH here, where both studies had a 71°C hot side and close cold side temperatures (13.9°C vs 13°C here), a porosity of 80%, and similar membrane widths (178 µm vs 200 µm here). This LMH figure is seen in Fig 10, after dividing out the membrane area inactivated by the feed support spacer (43% of area). Notably, the model here predicts an LMH of 49.8 °C, which is in good

agreement with their results. The results here are therefore both validated by the literature, and can sufficiently claim that superhydrophobic AGMD can be an improvement on the state-of-the-art.

The system was disassembled after the final 70 °C data point to examine the surface, which found mild flooding as seen in Fig 11**.**

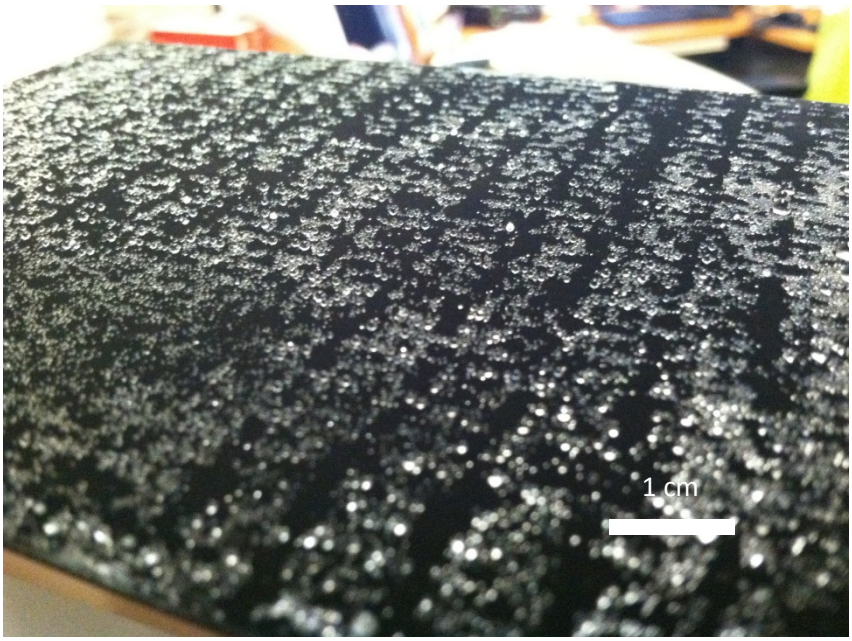

Fig. 11 Partially wetted superhydrophobic surface after high temperature condensation

Because of a high degree of pinning, the wetted droplets remained on the surface even when the surface was held upside down. One important implication of this test is that flooded conditions are not easily reversible [7]: once a surface becomes flooded, it remains that way even at conditions where flooding would not initiate. Drying is often necessary to remove the wetted droplets.

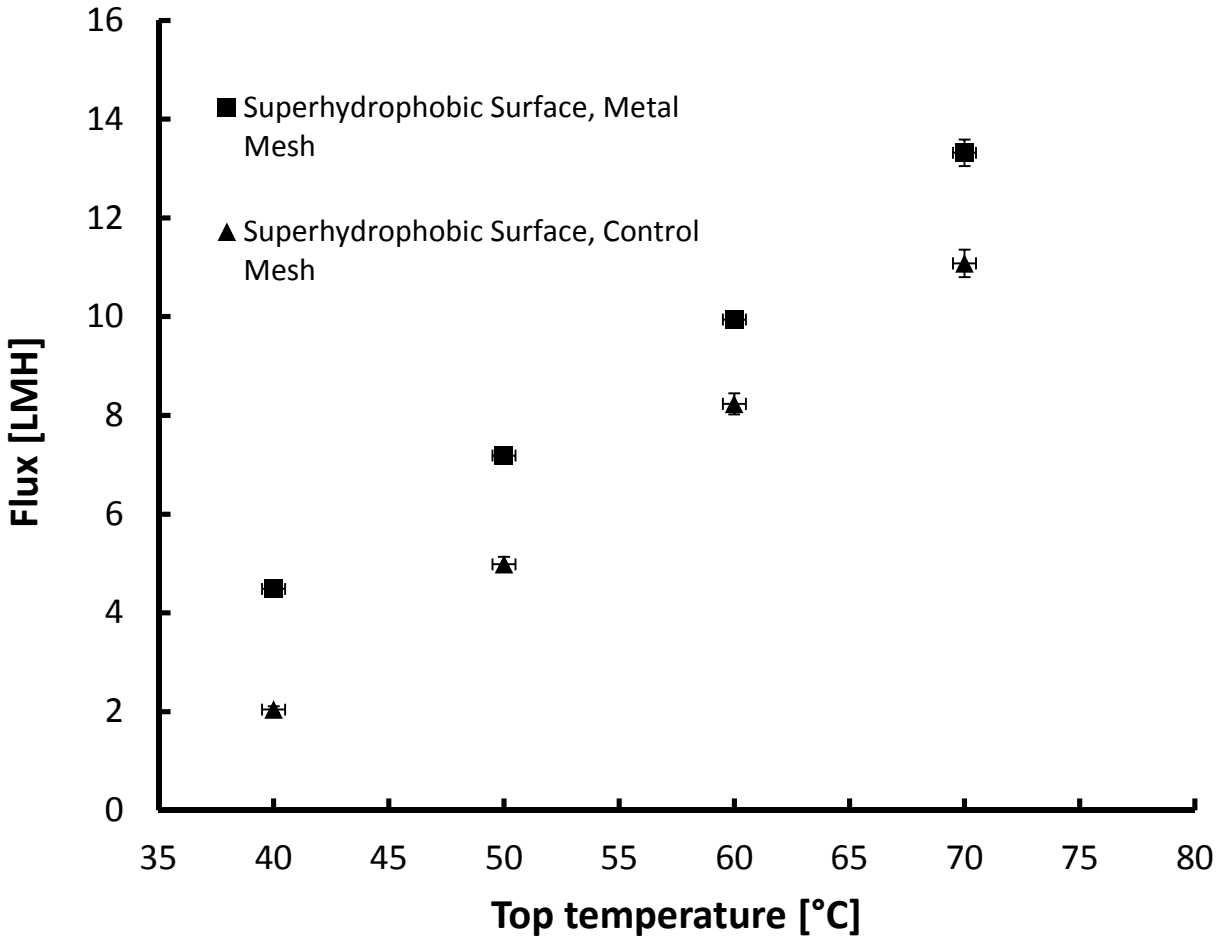

Fig. 12 Superhydrophobic condenser with highly conductive metal support mesh and a control mesh, ΔT =20°C between hot and cold channels. Conductivity of the stainless steel mesh: 16 W/mK. Conductivity of the plastic support mesh: 0.2 W/mK

Air gap membrane distillation, and most other forms of membrane distillation, generally requires a support structure to hold the thin, hydrophobic MD membranes in place. In these experiments, woven meshes were used, where 2/3 of the horizontal weaves were removed to minimize interference with condensation phenomena. In addition to hydrophobic experiments, use of a highly conductive mesh was of interest as a mechanism to reduce heat transfer resistance in the air gap, which generally has a large temperature difference. The conductive mesh improves heat conduction across the air gap, and acts as an additional condensing surface with a smaller effective air gap.

This increase in flux comes with a significant trade off: the metal mesh allows for more direct heat transfer between the hot channel and the cold channel, independent of vapor transport. While it is difficult to model the complex two phase hydrophobic condensing heat transfer, calculating the

adjusted effective conductivity of the gap, k_{gap}, can provide an estimate of thermal losses from the metal mesh.

In comparing experiments, it was found that the cold-side temperature did not have a significant impact on the distillate flux while the hot side temperature had a very significant effect: this agrees with previous studies [17].

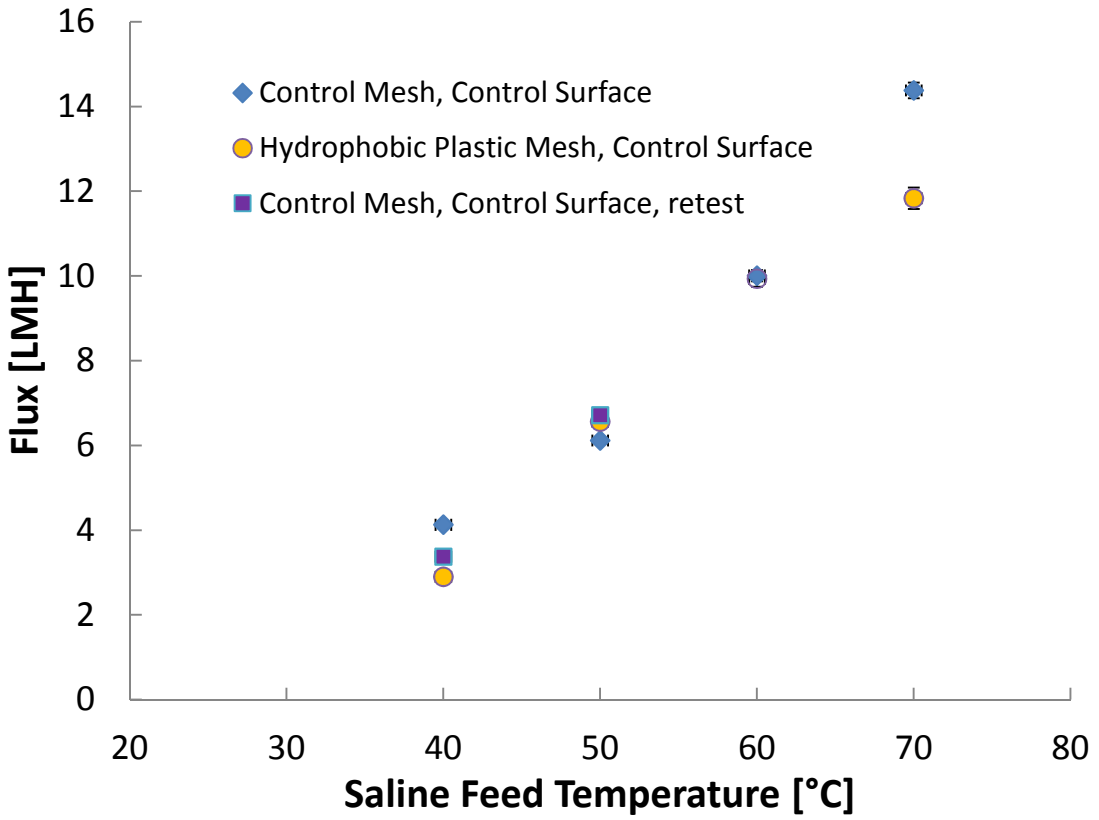

Fig. 13 Ordinary (hydrophillic condenser) AGMD on a copper control plate with varied support mesh hydrophobicity, ΔT =20°C between hot and cold channels.

The effect of the hydrophobicity of the support mesh on condensate production was also examined as a possible method for improving AGMD systems. Most AGMD models assume the effects of the mesh are relatively small and model the system as a laminar film on a flat surface. The results from the hydrophobic mesh experiment supported this approach, as making the mesh superhydrophobic with Neverwet® had a negligible effect on condensate production. A slight effect appeared at the 70 °C test point, which may be related to effects on flooding in the air gap, which began occurring in the system in these conditions around 65°C.

The results show that modifying the mesh spacer's conductivity had a significant effect on performance, but that its hydrophobicity did not. This occurs because the mesh does not act as a significant condensing surface unless its conductivity is very high. In the case of a metal support mesh, the mesh's conductivity was almost three orders of magnitude larger than that of the air in the gap, and two orders of magnitude larger than the conductivity of a plastic mesh. This agrees with previous studies have found that copper fins in the gap increase distillate flux [26].

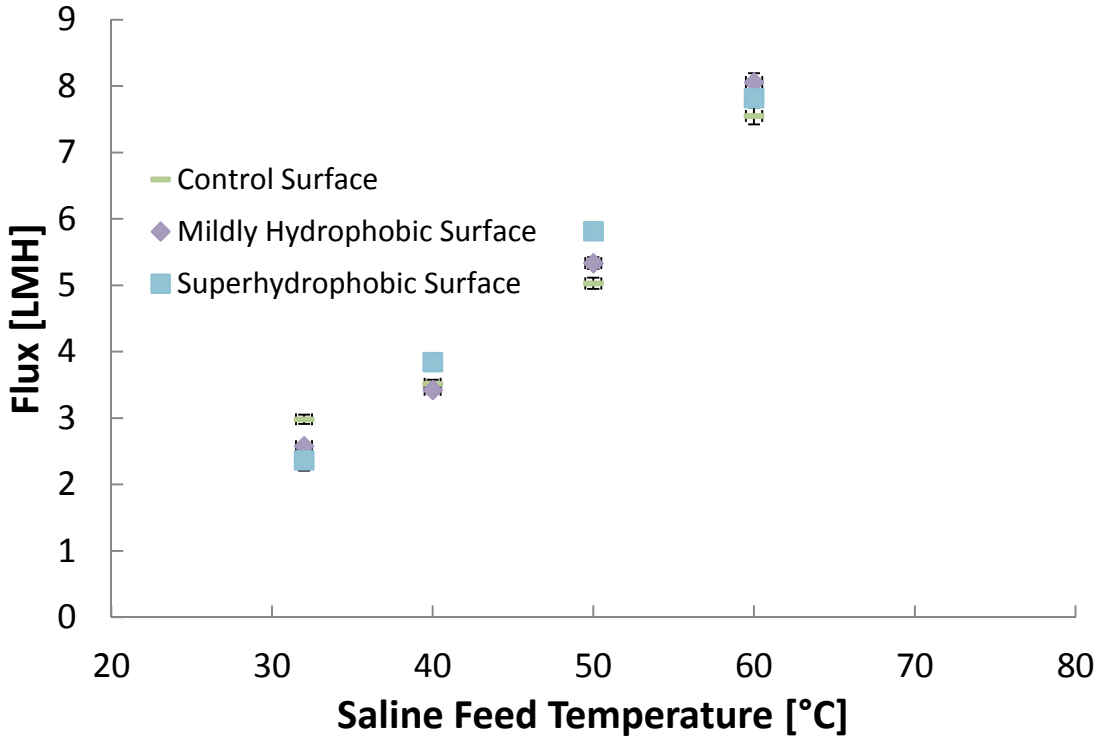

Fig. 14 Superhydrophobic, mildly hydrophobic, regular AGMD with a large air gap (1.5 mm), ΔT =20°C between hot and cold channels.

An experiment including both superhydrophobic and mildly hydrophobic surfaces was performed with a larger air gap. With this roughly three times larger air gap (1.5mm), the effect of superhydrophobic surfaces appeared to be greatly reduced. This result was possibly caused by the increased vapor diffusion resistance of the larger air gap and resulting lower flow rate of droplets, but hysteresis effects may also have been involved. Additionally, with the larger gap size, it is expected that flooding occurs less readily, but may still occur at the highest temperatures studied, which may explain the similar flux at 60°C. At this temperature, the flux of the mildly hydrophobic surface slightly outperforms the others. Under flooding conditions, superhydrophobic surfaces have a lower heat transfer rate than a smooth hydrophobic surface. Both undergo Wenzel drop-wise condensation, with

the superhydrophobic surface having larger, slower-moving drops due to a high degree of pinning which occurred as water infiltrated the rough copper oxide surface features.

However, unlike the others, this experiment was begun at a higher temperature for the superhydrophobic trial and then decreased, meaning that the detrimental effects of flooding may have continued down to lower temperatures. Such a result would indicate that superhydrophobic condensers might only be valuable in AGMD applications that operate within a certain range of conditions, and limit their usefulness in processes with a high peak flow rate and temperature difference.

Under most conditions the mildly hydrophobic plate performed similar to or better than the control plate, but did not outperform the superhydrophobic trial except under flooding conditions. The flux differences however remained relatively small. These results indicate that for larger air gaps, the beneficial effect of superhydrophobic surfaces on condensate production may be significantly reduced.

3.2 Comparison to Model

Simulations for a flooded gap, modeled as an elimination of air gap resistance and maximization of liquid film resistance, showed an increase in the rate of distillate flow. For the liquid gap case, the mass transfer coefficient and the distillate flux are higher compared to the air gap system, but at the expense of increased conductivity of the gap which reduces thermal efficiency. These results are seen in Fig 10.

In AGMD with jumping droplet condensation, the droplets may induce air circulation in the gap, leading to an improved heat and mass transfer coefficient and flux due to reduced air gap resistance. Due to rapid shedding of droplets at small diameters, the heat and mass transfer resistances of the condensate film are also reduced nearly to zero.

Due to the dynamics of a jumping droplet, the effective air gap thickness as modeled may be reduced. Droplets eject from the condenser surface and enter the air gap. For a horizontal air gap as used in our system, droplets will fall in towards the membrane and downwards. During this flight, the droplet's distance from the membrane is reduced which leads to a reduction in mass flow resistance. Because the droplet remains at a lower temperature than the air near the membrane, condensation will continue to occur on the droplet as it falls. Droplets may bounce off of the membrane and continue their flight with minimal heat transfer losses.

The jumping droplets may adhere to the hydrophobic membrane after ejection from the condenser plate. Initially when this occurs and the droplet temperature is still near the temperature of the condensing surface, it behaves as a locally flooded system, which increases distillate flux. Due to its small size, the temperature of the drop quickly approaches the temperature of the membrane and the rate of condensation is significantly reduced. When gravitational forces on the adhered droplet become significant compared to the surface-energy adhesion forces (Bond number >0.1-1 depending on surface hydrophobicity [27]), the droplet will fall down the membrane surface readily, as in standard drop-wise condensation.

In the case of flooded Wenzel droplets strongly adhering (pinning) to the superhydrophobic surface, which can occur in regimes of high condensate flux, the flooded droplets become large compared to the

gap size (1 mm), touching the membrane. Thus the air gap width becomes locally zero in some places, improving distillate flux as seen in the flux equation and experiments. These larger flooded droplets are also responsible for thermal bridging between the condenser and membrane, which decreases resistance to heat flow and reduces the thermal efficiency of the system.

A comparison was made between the results of the jumping droplet experiment and the model for fully flooded air gap conditions, which is a simplification of the condensate flow model where the condensate film thickness becomes the entire width of the air gap. Jumping droplet condensation was found to have close-to but inferior condensate production when compared to the flooded gap and significantly higher flux than the ordinary AGMD model. Though this work did not include a direct model for jumping droplet condensation, which would involve an under-constrained two phase flow problem, the comparison to the standard and flooded AGMD models demonstrated the ability for superhydrophobic condensers in AGMD to minimize mass transfer resistance.

4. CONCLUSIONS

Superhydrophobic condensing surfaces have shown very significant distillate flux increases for AGMD, with more than a 100% improvement in some cases. However, at high heat transfer rates, the benefit of superhydrophobic surfaces becomes negligible. Visual validation confirmed that flooding and large droplet pinning occurred on the superhydrophobic surface at these high heat transfer rates, and confirmed that jumping droplet condensation occurred at lower heat transfer rates. This result is in line with past studies of superhydrophobic surfaces which showed a transition to flooding at high heat transfer rates. The temperature differences in realistic membrane distillation configurations are smaller (<10°C) than those studied here, and fit within the range of heat transfer rates where jumping droplet condensation provides significant benefit.

The hydrophobicity of the support mesh for the membrane was found to have minimal effect on the distillate flow rate, but high conductivity for the mesh showed notable improvement in distillate flux. Jumping droplet and wetted drop-wise condensation increase the mass transfer coefficient in the air gap, resulting in higher distillate flux and reduced temperature gradients within the condensate. Numerical modeling with EES accurately represented cases with film condensation and the EES model with no air gap resistance reasonably approximated the distillate production of superhydrophobic condensation, indicating that this jumping-droplet condensation significantly reduces the effective heat and mass transfer resistances of the air gap. Thus the mass transfer resistance behavior was similar to a flooded gap system, but without the conductive losses of a flooded gap.

AGMD is the membrane distillation configuration with the smallest sensible heat loss, and superhydrophobic condensation surfaces may be a valuable tool to further improve efficiency and the rate of distillate production in AGMD systems. Further work should be performed to accurately model the dynamics of jumping droplet condensation in AGMD and to compare the thermal efficiencies of AGMD using various condenser treatments, as well as flooded gap efficiency to quantify these values.

ACKNOWLEDGEMENT

This work was funded by the Cooperative Agreement Between the Masdar Institute of Science and Technology (Masdar University), Abu Dhabi, UAE and the Massachusetts Institute of Technology (MIT), Cambridge, MA, USA, Reference No. 02/MI/MI/CP/11/07633/GEN/G/00.

References

[1] D. M. Warsinger, J. Swaminathan, E. Guillen-Burrieza, H. A. Arafat, and J. H. Lienhard V, "Scaling and fouling in membrane distillation for desalination applications: A review," *Desalination*, vol. 356, 2014.

[2] J. Gilron, L. Song, and K. K. Sirkar, "Design for cascade of crossflow direct contact membrane distillation," *Industrial & Engineering Chemistry Research*, vol. 46, no. 8, pp. 2324–2334, 2007.

[3] H. Lee, F. He, L. Song, J. Gilron, and K. K. Sirkar, "Desalination with a cascade of cross-flow hollow fiber membrane distillation devices integrated with a heat exchanger," *AIChE Journal*, vol. 57, no. 7, pp. 1780–1795, 2011.

[4] F. He, J. Gilron, and K. K. Sirkar, "High water recovery in direct contact membrane distillation using a series of cascades," *Desalination*, vol. 323, pp. 48–54, 2013.

[5] E. K. Summers and J. H. Lienhard V, "Experimental study of thermal performance in air gap membrane distillation systems including direct solar heating of membranes," *Desalination*, vol. 330, pp. 100–110, 2013.

[6] E. K. Summers, H. A. Arafat, and J. H. Lienhard V, "Energy efficiency comparison of single-stage membrane distillation (MD) desalination cycles in different configurations," *Desalination*, vol. 290, pp. 54–66, 2012.

[7] A. Lafuma and D. Quere, "Superhydrophobic states," *Nature Materials*, vol. 2, pp. 457–460, 2003.

[8] R. N. Wenzel, "Resistance of solid surfaces to wetting by water," *Industrial & Engineering Chemistry*, vol. 28, pp. 988–994, 1936.

[9] A. B. D. Cassie and S. Baxter, "Wettability of porous surfaces," *Transactions of the Faraday Society*, vol. 40, pp. 546–551, 1944.

[10] D. Quere, "Wetting and roughness," *Annual Review of Materials Research*, vol. 38, pp. 71–99, 2008.

[11] N. Miljkovic and E. N. Wang, "Condensation heat transfer on superhydrophobic surfaces," *Materials Research Society*, vol. 38, pp. 397–406, 2013.

[12] D. H. Kim, B. M. Jenkins, and J. H. Oh, “Gypsum scale reduction and collection from drainage water in solar concentration,” *Desalination*, vol. 265, no. 1-3, pp. 140–147, 2011.

[13] R. Chouikh and S. Bouguecha, “Modelling of a modified air gap distillation membrane for the desalination of seawater,” vol. 181, pp. 257–265, 2005.

[14] G. L. Liu, C. Zhu, C. S. Cheung, and C. W. Leung, “Theoretical and experimental studies on air gap membrane distillation,” *Heat and Mass Transfer*, vol. 34, no. 4, pp. 329–335, 1998.

[15] N. Miljkovic, R. Enright, Y. Nam, N. Lopez, Ken an Dou, J. Sack, and E. N. Wang, “Jumping-droplet-enhanced condensation on scalable superhydrophobic nanostructured surfaces,” *Nanoletters*, vol. 13, pp. 179–187, 2012.

[16] S.A.Klein, “Engineering equation solver version 9.”

[17] M. Khayet and C. Cojocaru, “Air gap membrane distillation: Desalination, modeling and optimization,” *Desalination*, vol. 287, no. 0, pp. 138 – 145, 2012. Special Issue in honour of Professor Takeshi Matsuura on his 75th Birthday.

[18] R. Leslie, A. Elmoursi, R. Gazdecki, and S. Oneufer, “Coating compositions and methods for coating network protector and safety switch housings,” May 16 2013. US Patent App. 13/670,545.

[19] C. Fernández-Pineda, M. A. Izquierdo-Gil, and M. Garca-Payo, “Gas permeation and direct contact membrane distillation experiments and their analysis using different models,” *Journal of Membrane Science*, vol. 198, no. 1, pp. 33–49, 2002.

[20] A. Mills, *Heat Transfer 2nd Edition*. Prentice Hall, 1998.

[21] E. K. Summers and J. H. Lienhard V, “A novel solar-driven air gap membrane distillation system,” *Desalination and Water Treatment*, vol. 51, pp. 1–8, 2012.

[22] D. E. M. Warsinger, J. Swaminathan, and J. H. Lienhard V, “Effect of module inclination angle on air gap membrane distillation,” in *Proceedings of the 15th International Heat Transfer Conference, IHTC-15, Paper No. IHTC15-9351*, Kyoto, Japan August 2014.

[23] R. Enright, N. Miljkovic, and E. N. Wang, “Condensation on superhydrophobic copper oxide nanostructures,” *Journal of Heat Transfer*, vol. 135, 2013.

[24] J. H. Lienhard V and J. H. Lienhard IV, *A Heat Transfer Textbook Fourth Edition*. Dover Publications, Inc, 2011.

[25] N. Miljkovic, R. Enright, and E. N. Wang, “Effect of droplet morphology on growth dynamics and heat transfer during condensation on superhydrophobic nanostructured surfaces,” *ASC Nano*, vol. 6, pp. 1776–1785, 2012.

[26] L.-H. Cheng, Y.-H. Lin, and J. Chen, “Enhanced air gap membrane desalination by novel finned tubular membrane modules,” *Journal of Membrane Science*, vol. 378, no. 1, pp. 398–406, 2011.

[27] C.-W. Lo, C.-C. Wang, and M.-C. Lu, “Scale effect on dropwise condensation on superhydrophobic surfaces,” *ACS applied materials & interfaces*, vol. 6, no. 16, pp. 14353–14359, 2014.